Electrochemistry Communications 106 (2019) 106512

Contents lists available at ScienceDirect

Electrochemistry Communications

journal homepage: www.elsevier.com/locate/elecom

Short communication

Proving insertion of Mg in Mn_2O_3 electrodes through a spectroelectrochemical study

Carmen Miralles, Roberto Gómez*

Departament de Química Física i Institut Universitari d'Electroquímica, Universitat d'Alacant, Apartat 99, E-03080 Alicante, Spain

ARTICLE INFO

Keywords:
Magnesium battery
Mn_2O_3 microcubes
UV–vis spectroelectrochemistry
Magnesium insertion
Organic electrolyte

ABSTRACT

The scarcity of lithium in the Earth's crust makes advisable to look for batteries alternative to those of Li-ion. Magnesium batteries are suitable candidates as this metal is abundant. In this context, Mn (III) oxide is a material that could be used for the insertion of magnesium ions. Mn_2O_3 thin electrodes were synthesized for the first time through a hydrothermal procedure followed by heat treatment. Through cyclic voltammetry (CV) and spectroelectrochemical (UV–vis) techniques together with ex situ XPS analysis, the effective insertion of magnesium in the Mn_2O_3 lattice is demonstrated, which means that this material could be used as a cathode in Mg batteries. Finally, the need for nanostructuring is highlighted for practical applications.

1. Introduction

The continuous increase in energy demand makes it essential to manufacture secondary batteries capable of accumulating the energy generated from renewable energy sources. In the future, one of the applications of these batteries could be to supply power to the grid when production does not meet the demand. This would facilitate that the energy consumption in households is clean and sustainable.

Lithium-ion batteries are practical, because of their high energy density together with remarkable power density [1]. From a purely technical point of view, the Li-ion battery would be chosen to accumulate energy from renewable energy sources. However, this battery has the disadvantage that the reserves of lithium in the planet are finite and very localized [2]. In addition, it is uncertain that there is enough available lithium to supply all the energy needs of the highly technological world to which we are heading. For this reason, it is necessary to investigate batteries made up of metals more abundant in the Earth's crust, such as Mg.

The main potential advantages of magnesium with respect to lithium are: i) it is divalent while lithium is monovalent and, as a result, it has a higher volumetric capacity than lithium (Mg: 3833 $mA{\cdot}h{\cdot}cm^{-3}$, Li: 2062 $mA{\cdot}h{\cdot}cm^{-3}$); ii) it is more environmentally benign; iii) it is approximately three orders of magnitude more abundant in weight than Li [3]. However, Mg has two main drawbacks: a slow insertion kinetics in the cathode materials studied to date and a lack of electrolytes in which both electrodeposition and insertion processes for magnesium are reversible and compatible. In addition, it has been recently demonstrated that magnesium deposition can lead to the formation of dendrites depending on the experimental conditions and the type of electrolyte [4] in contrast with previous understanding [5,6].

There are numerous types of cathode materials that have been studied for magnesium batteries. Among them we find sulfides (Mo_6S_8 [7], MoS_2 [8] and Ti_2S_4 [9]) and binary (MnO_2 [10], MoO_3 [11] and V_2O_5 [12]) and ternary oxides ($MgMn_2O_4$ [13]). The family of MnO_2 is characterized by the variety of polymorphs with both open (with tunnels) and laminar structures (α-MnO_2 hollandite, todorokite and birnessite). Despite the good gravimetric capacities of some polymorphs, they have not shown acceptable cycling stability and therefore it is necessary to investigate other oxides [14]. In this work, we propose Mn_2O_3 as a cathode electrode material for Mg-based batteries. The reasons why we have chosen this material are: i) it is related to the oxides of the MnO_2 family; ii) it is a material rather extensively studied in the context of lithium batteries due to its good physicochemical characteristics (thermal stability, non-toxicity and a high theoretical capacity of 1018 $mA{\cdot}h{\cdot}g^{-1}$) [15,16]; iii) there is a precedent for the insertion of a divalent cation, such as Zn^{2+} in its structure [17]. The most stable polymorph of Mn_2O_3 is bixbyite, with a rather open structure, which facilitates cation insertion. In fact, the bixbyite structure can be considered as an anion deficient fluorite structure.

As far as we know, Mn_2O_3 only appears listed without any details in a table for magnesium insertion materials contained in an article from 1990 [18]. Thus it remains virtually unexplored in the context of magnesium batteries. It seems thus timely to study the insertion of magnesium in this material in more depth and to evaluate its potential application in the context of magnesium batteries.

* Corresponding author.
E-mail address: roberto.gomez@ua.es (R. Gómez).

https://doi.org/10.1016/j.elecom.2019.106512
Received 9 June 2019; Received in revised form 30 July 2019; Accepted 11 August 2019
Available online 12 August 2019

2. Materials and methods

10 mmol of $MnCl_2{\cdot}4H_2O$ and 50 mmol of urea were dissolved in two separate flasks. Then, 5 ml of each solution was added to a pressure-resistant glass bottle containing either stainless steel or F:SnO_2 (FTO) conducting glass substrates. The bottle was maintained in an oven at 90 °C for 5 h. Finally, the electrodes were submitted to a heat treatment at 550 °C for 10 h in air. The procedure to synthesize Mn_2O_3 as thin films on FTO conducting glass substrates is the same, although the hydrothermal treatment was limited to 1 h 25 min. The loading of the substrate with Mn_2O_3 attained a value of 1.64 mg cm^{-2}.

The Mn_2O_3 electrodes were electrochemically characterized by cyclic voltammetry (CV) in a three-electrode two-compartment cell by means of a computer controlled AUTOLAB PGSTAT30 potentiostat. In aqueous media (0.1 M $MgCl_2$), an FTO/Mn_2O_3 electrode was used as a working electrode, a Pt wire as a counter-electrode and an Ag/AgCl/KCl (3 M) as a reference electrode. In organic media (0.5 M $Mg(ClO_4)_2$ in acetonitrile (AN)), a SS/Mn_2O_3 electrode was used as a working electrode and Mg wires as counter- and reference electrodes.

The crystal structure of Mn_2O_3 was identified by X-ray Diffraction obtained with a Bruker D8-Advance instrument by using Cu K radiation (40 kV and 40 mA) in the 2θ range from 20° to 70° using 1° min^{-1} as a step scan. The XPS spectra were recorded by a Thermo-Scientific K-Alpha XPS spectrometer equipped with a monochromatic Al—K source operating at 15 kV and 10 mA. Analysis with XPS was performed before and after ion etching. The morphology of Mn_2O_3 deposits was analyzed using a ZEISS Merlin VP Compact Field Emission Scanning Electron Microscope (FE-SEM).

Spectroelectrochemical experiments were performed with a Shimadzu UV-2401PC, UV–vis spectrophotometer with electrochemical control through a micro-Autolab potentiostat. The electrochemical cell for spectroelectrochemical experiments was equipped with a glass cuvette with a 1 cm optical path length. Mn_2O_3 thin films deposited on FTO were used as working electrodes, a Pt wire as a counter electrode and a commercial Ag/AgCl/KCl (3 M) as a reference electrode.

3. Results and discussion

The crystalline structure and morphology of Mn_2O_3 were analyzed by XRD and FE-SEM techniques. As we can see in Fig. 1, all the peaks that appear in the X-Ray diffractogram are ascribed to the Mn_2O_3 cubic structure. These peaks and their corresponding plane reflections are: 23.1°, (211); 33.0°, (222); 38.3°, (400); 45.3°, (332); 49.3°, (431); 55.2°, (440); 65.8°, (622). The morphology of the deposit of Mn_2O_3 shows a rather compact microstructure with cubic crystals (Fig. 2a) whose facets are porous (Fig. 2b). The average size of the cubes is 3.2 μm.

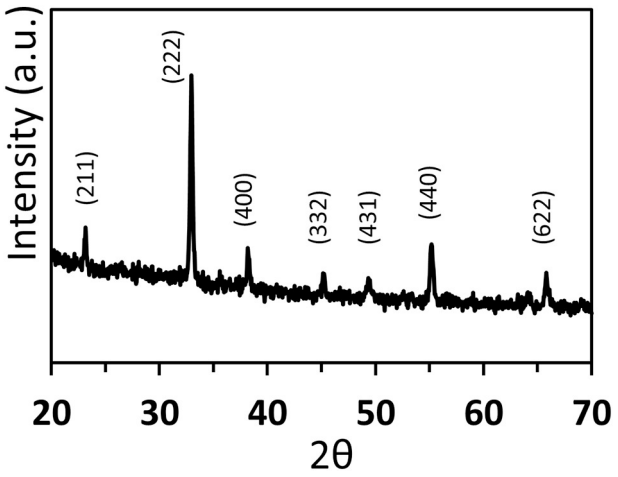

Fig. 1. XRD pattern for Mn_2O_3 powder.

The study of the insertion of magnesium in Mn_2O_3 was carried out in both organic and aqueous media. The results obtained in both cases help to confirm Mg insertion regardless of the nature of the solvent. However, in aqueous media, the insertion of protons from water in the cathode could also be envisaged. This has been demonstrated to be the case for V_2O_5 [19,20] and MnO_2 [21] cathode materials. Fig. 3a,b shows voltammetric profiles obtained at 5 mV s^{-1} in aqueous and organic media respectively, revealing both a quasi-reversible pseudo-capacitive response although in the organic medium an irreversible cathodic contribution is apparent in the low potential region.

To provide direct evidence for Mg insertion, XPS analysis both at the surface level and after etching have been carried out. Fig. 3 a1, a2, b1 and b2 show the Mg 1 s spectral region for electrodes emerged at the potential window limits for both aqueous and organic media. As observed in Fig. 3, when the electrode material is reduced (Fig. 3 a1 and b1), the XPS Mg 1s signal (both at the surface sample and after etching) is significantly more intense than for the oxidized state (Fig. 3 a2 and b2). This clearly indicates that magnesium ions are either adsorbed and/or inserted in the Mn_2O_3 lattice. The difference in intensity prior and after etching is minor, which point to the fact that Mg^{2+} insertion rather than simple adsorption accounts for the electrochemical and spectroscopic results. Therefore, from the XPS and CV results, the pseudo-capacitive signals can be ascribed to magnesium insertion in both media. X-ray diffractograms were also acquired for electrodes emerged at the potential window limits. Both were virtually identical to that shown in Fig. 1 for the freshly prepared material. This observation suggests Mn_2O_3 to be an insertion rather than a conversion electrode material, although the low degree of material utilization could also explain this observation (see below).

In addition, we can see in Fig. 3 that, in the case of the aqueous medium, surface analysis demonstrates virtually complete magnesium de-intercalation at positive potentials, which indicates that the intercalation process is close to fully reversible. In any case, the etched sample still shows a weak signal for Mg, which reveals that a minor part of the intercalated magnesium remains in the inner part of the Mn_2O_3 crystals, while it is fully removed in the outermost part. In the case of the organic medium, the difference in intensity of the Mg 1s XPS signals between the reduced and the oxidized states is much smaller than in aqueous medium, uncovering the largely irreversible character of the process [22]. This agrees with the electrochemical behavior observed in Fig. 3b, in which net irreversible cathodic currents are recorded below 1.3 V vs. Mg^{2+}/Mg. The poor de-insertion of Mg in organic medium could be due to the way in which Mg^{2+} ions are coordinated with the solvent and the anionic species presents in the electrolyte [23,24]. In contrast, in aqueous media, the participation of hydrated species and hydroxo/aquo-complexes is anticipated [25]. These species would insert with Mg ion in the Mn_2O_3 lattice. This phenomenon is called co-insertion and it would facilitate the de-insertion of Mg [20,26]. The significant difference between both media is also reflected in the potential window at which the insertion process occurs. The corresponding voltammetric signals appear at more positive potentials (vs. Mg^{2+}/Mg) in aqueous media.

It is worth noting that the charge exchanged in the CVs is rather modest. From the cathodic charge associated with magnesium insertion, we have calculated the capacity of Mn_2O_3 in aqueous media, resulting a value as low as 2.8 mA h g^{-1}. This indicates that magnesium insertion only affects the outermost layer of the material, the bulk being electrochemically inactive. If we assume that the value of theoretical capacity is equal to 224 mA·h·g^{-1} as given by Winterton and coworkers [18], only 1.3% of the material would be being utilized. In our case, the deposit contained 1.64 mg cm^{-2}. Knowing the density of Mn_2O_3 (4.5 g cm^{-3}), we can calculate the thickness of the material that is actually working. This thickness is 45 nm and the total thickness of the Mn_2O_3 deposit is 3.6 μm. In the calculation of the magnesium insertion depth, a roughness factor equal to one is considered. If we consider a

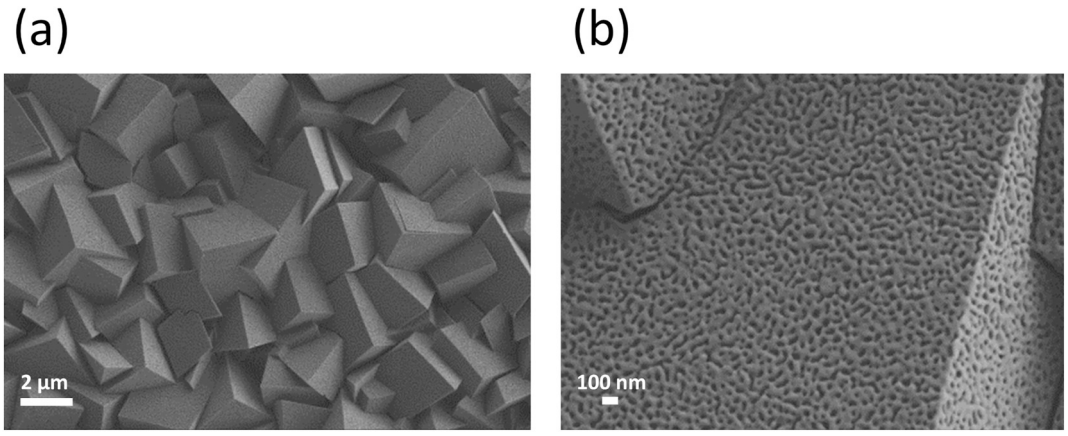

Fig. 2. a) and b) FE-SEM images of the surface of a Mn_2O_3 deposit at different magnifications.

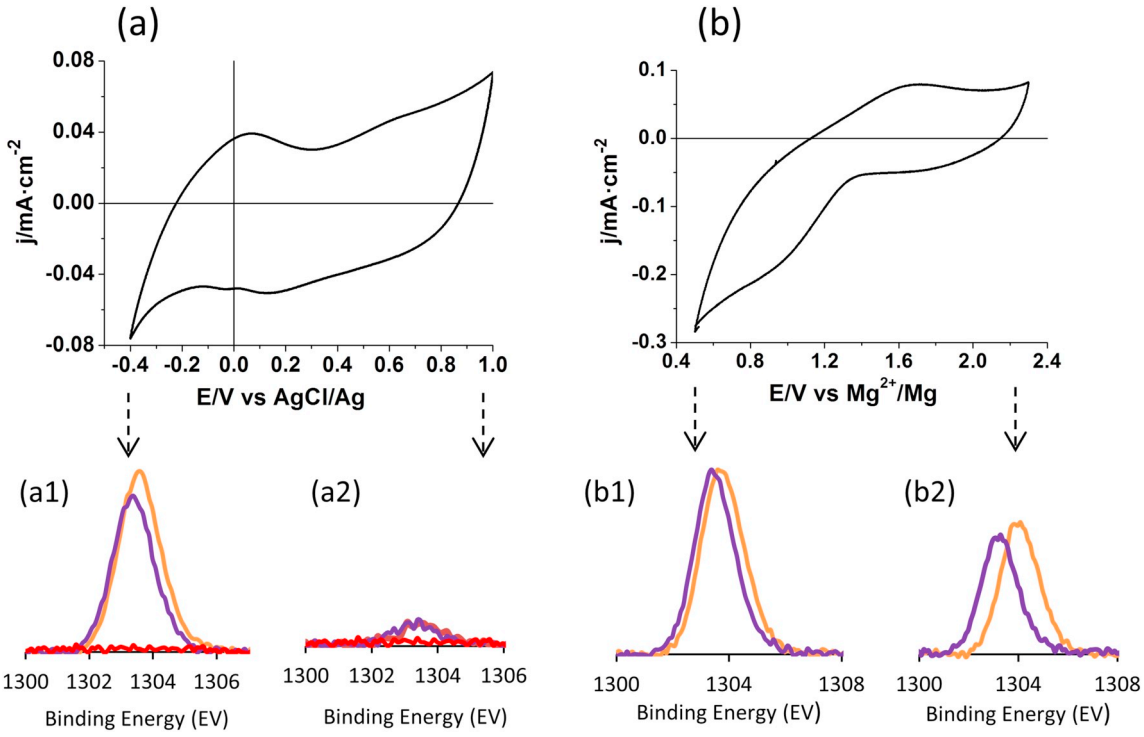

Fig. 3. a) CV for FTO/Mn_2O_3 in 0.1 M of $MgCl_2$; a1) and a2) Mg 1s spectra when the electrode is reduced at −0.4 V (a1) and when it is oxidized at 1.0 V (a2); b) CV for SS/Mn_2O_3 in 0.5 M of $Mg(ClO_4)_2$ in acetonitrile; b1) and b2) XPS pattern of Mg 1s when the electrode is reduced at 0.5 V vs. Mg^{2+}/Mg (2a) and when it is oxidized at 2.3 V vs. Mg^{2+}/Mg. The orange line corresponds to a surface analysis, the violet line to the etched sample and the red line to a freshly prepared sample. (For interpretation of the references to color in this figure legend, the reader is referred to the web version of this article.)

minimum roughness factor of $\sqrt{3}$, an insertion thickness of 25 nm would be calculated.

The mechanism of Mg insertion in the Mn_2O_3 lattice is probably similar to that of Zn^{2+} due to the fact that both metals are divalent and their ionic radii are similar, 74 pm (Zn^{2+}) and 72 pm (Mg^{2+}). As reported by Jiang et al. [17] for Zn insertion, Mn_2O_3 is initially present in the bixbyite phase and, after Zn insertion, it is transformed into the birnessite phase (laminar). The insertion process may be represented by:

$$Mn_2O_3 + xZn^{2+} + 2xe \rightleftarrows Zn_xMn_2O_3 \quad (1)$$

Analogously, we proposed the following equation for Mg insertion in Mn_2O_3:

$$Mn_2O_3 + xMg^{2+} + 2xe \rightleftarrows Mg_xMn_2O_3 \quad (2)$$

The $Mg_xMn_2O_3$ ternary oxide (where $x < 1$) has Mn in both II and III oxidation states and thus it may be denoted as $Mg_xMn(III)_{2-2x}Mn(II)_{2x}O_3$. These equations are simplified versions of the complex processes occurring during insertion, which may entail manganese dissolution and precipitation as well as proton insertion. This complexity is aggravated by the rich chemistry of manganese and the possibility of proton insertion.

UV–vis spectroelectrochemical analysis (employing cyclic voltammetry) was carried out to complement the electrochemical study of Mn_2O_3. It is known that MnO_2 is weakly electrochromic as its color slightly changes depending on the Mn oxidation state [27]. It is expected that this behavior can be extrapolated to Mn_2O_3 and used for studying magnesium insertion. Taking into account that Mn_2O_3 is black, while Mn(II) (hydr)oxides are either green (MnO) or white ($Mn(OH)_2$), one would expect that Mg insertion, which leads to a partial

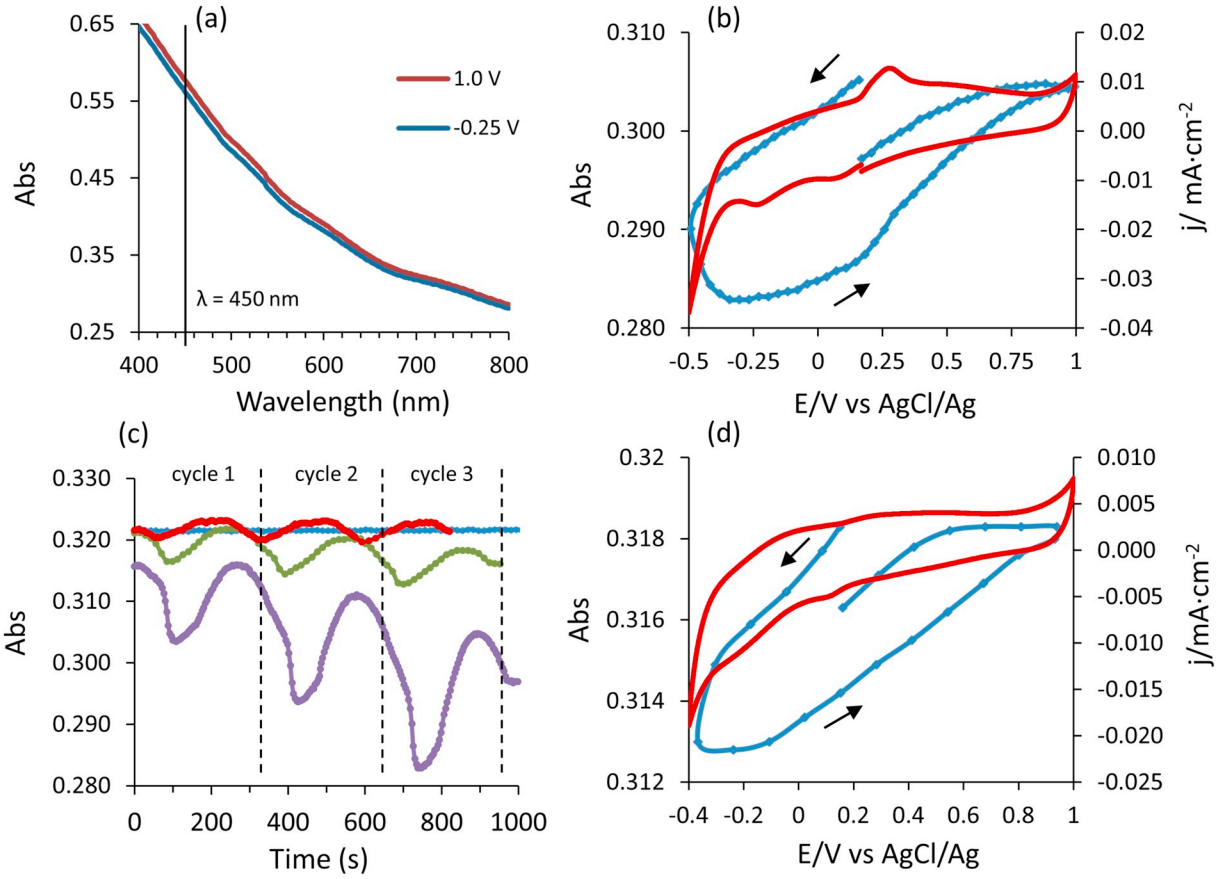

Fig. 4. (a) Visible adsorption spectra for Mn_2O_3 thin films in 0.1 M of $MgCl_2$ at −0.25 V (blue) and 1.0 V (red), (b) and (d) cyclic voltammograms of Mn_2O_3 thin films in 0.1 M of $MgCl_2$ coupled with absorption spectroscopy experiments in the visible range. The red line denotes the CV and the blue one the change in absorbance at λ = 450 nm. (c) Variation of absorbance versus time at λ = 450 nm for different potential windows, (−0.25–1.0 V) red, (−0.4–1.0 V) green, (−0.5–1.0 V) violet and at 0.2 V (blue), which is within the redox stability potential. Dashed lines delimit the different cycles. (For interpretation of the references to color in this figure legend, the reader is referred to the web version of this article.)

conversion of Mn(III) to Mn(II), is accompanied by a bleaching of the electrode. UV–vis spectra were acquired in the range from 400 to 800 nm at different potentials to identify a wavelength providing sufficient coloration contrast in the potential window in which Mg insertion occurs. Fig. 4a shows spectra taken at 1.0 V and −0.25 V. As expected, absorbance is slightly but consistently lower at −0.25 V, pointing to the presence of Mn (II). The difference between the absorbance at both potentials has a maximum at 450 nm, which is thus the wavelength chosen for the spectroelectrochemical monitoring of Mg insertion.

An important aspect of the behavior of Mn_2O_3 electrodes is their reversibility (and stability) particularly as a function of the employed potential window. Fig. 4b shows simultaneously acquired absorbance (blue line) and current density (red line) versus applied potential in the course of a CV in the potential window from −0.5 to 1.0 V. It is remarkable that the initial and final absorbance after one complete cycle do not coincide presumably because of the existence of an irreversible process that could be linked to partial dissolution of the oxide. Such an irreversible process is also reflected in the corresponding CV, which exhibits a sudden increase in the cathodic current densities at potentials below −0.4 V. To check the effect of the negative potential limit on the spectroelectrochemical behavior of the Mn_2O_3 electrodes, the absorbance was monitored versus time in the course of three voltammetric cycles with variable negative limits (−0.25 V, −0.40 V and −0.50 V) as shown in Fig. 4c.

The potential window in which Mn_2O_3 has a reversible electrochemical behavior goes from −0.25 to 1.0 V as confirmed by the fact that the initial and final absorbance values coincide. This is not the case for more negative values (−0.4 and, particularly, −0.5 V), in which a cycle-by-cycle decay of the absorbance is observed. This is probably linked to a partial dissolution of the oxide as Mn(II) in the aqueous electrolyte [28]. Fig. 4d shows the absorbance and current density vs. potential when the negative limit is of −0.4 V. Interestingly, the hysteresis in the absorbance plot is accompanied by the development of negative currents at potentials close to the negative limit, which would be linked to the reduction to Mn(II).

4. Conclusions

In conclusion, we have synthesized Mn_2O_3 thin films on conducting glass through a chemical bath deposition method and we have subsequently carried out a spectroelectrochemical study aiming to evaluate the ability of this material to insert magnesium ions. We have shown that both in aqueous and in organic media, magnesium ion insertion in the Mn_2O_3 lattice takes place. The UV–vis spectroelectrochemical measurements demonstrate that, in aqueous media, Mn_2O_3 has a quasi-reversible performance in potential window between −0.25 and 1.0 V. In any case, from a practical point of view, both nanostructuring of Mn_2O_3 and an increase in electrode porosity are needed as a way to increase the low current densities recorded in both aqueous and organic media and thus, low electrode capacity. In fact, nanostructuring (below 50 nm in characteristic size) would allow us to increase the surface area and decrease the ionic diffusion length, which is beneficial for the kinetics of the insertion/de-insertion process because the average distance that the magnesium ions need to travel is much shorter than in more compact materials [29,30]. In addition, for optimizing the

behavior of the electrodes, the use of conductive additive and binder should be considered.

Acknowledgements

This work has been supported by the Spanish Ministry of Science, Innovation and Universities through projects MAT2015-71727 and RTI2018-102061-B-I00 (FONDOS FEDER). C.M. Is grateful to the Vicepresidency of Research and Innovation of the University of Alicante for the award of an FPU grant.

References

[1] D. Linden, T.B. Reddy, Handbook of Batteries, 4 th ed., McGraw-Hill, New York, 2011.
[2] H.D. Yoo, I. Shterenberg, Y. Gofer, G. Gershinsky, N. Pour, D. Aurbach, Energy Environ. Sci. 6 (2013) 2265–2279 https://doi.org/10.1039/c3ee40871j.
[3] A.A. Yaroshevsky, Geochem. Int. 44 (2006) 48–55, https://doi.org/10.1134/S001670290601006X.
[4] R. Davidson, A. Verma, D. Santos, F. Hao, C. Fincher, S. Xiang, J.V. Buskirk, K. Xie, M. Pharr, P.P. Mukherjee, S. Banerjee, ACS Energy Lett 4 (2019) 375–376, https://doi.org/10.1021/acsenergylett.8b02470.
[5] M. Masaki, J. Power Sources 196 (2011) 7048–7055, https://doi.org/10.1016/j.jpowsour.2010.11.141.
[6] D. Aurbach, Y. Cohen, M. Moshkovich, Electrochem. Solid-State Lett. 4 (2001) A113–A116, https://doi.org/10.1149/1.1379828.
[7] M. Levi, H. Gizbar, E. Lancry, Y. Gofer, E. Levi, D. Aurbach, J. Electroanal. Chem. 569 (2004) 211–223, https://doi.org/10.1016/j.jelechem.2004.03.004.
[8] Y. Liang, H.D. Yoo, Y. Li, J. Shuai, H.A. Calderon, F.C.R. Hernandez, L.C. Grabow, Y. Yao, Nano Lett. 15 (2015) 2194–2202, https://doi.org/10.1021/acs.nanolett.5b00388.
[9] X. Sun, P. Bonnick, V. Duffort, M. Liu, Z. Rong, K.A. Persson, G. Cederd, L.F. Nazar, Energy Environ. Sci. 9 (2016) 2273–2277, https://doi.org/10.1039/c6ee00724d.
[10] C. Ling, R. Zhang, T.S. Arthur, F. Mizuno, Chem. Mater. 27 (2015) 5799–5807, https://doi.org/10.1021/acs.chemmater.5b02488.
[11] G. Gershinsky, H.D. Yoo, Y. Gofer, D. Aurbach, Langmuir 29 (2013) 10964–10972, https://doi.org/10.1021/la402391f.
[12] X. Du, G. Huang, Y. Qin, L. Wang, RSC Adv. 5 (2015) 76352–76355, https://doi.org/10.1039/c5ra15284d.
[13] G. Liu, Q. Chi, Y. Zhang, Q. Chen, C. Zhang, K. Zhub, D. Cao, Chem. Commun. 54 (2018) 9474–9477, https://doi.org/10.1039/c8cc05366a.
[14] R. Zang, T.S. Arthur, C. Ling, F. Mizuno, J. Power Sources 282 (2015) 630–638, https://doi.org/10.1016/j.jpowsour.2015.02.067.
[15] S.Z. Huang, J. Jin, Y. Cai, Y. Li, Z. Deng, J.Y. Zeng, C.J. Liu, C. Wang, T. Hasan, B.L. Su, Sci. Rep. 5 (2015) 14686, , https://doi.org/10.1038/srep14686.
[16] Y.C. Zhang, J.T. Li, C.G. Wu, L. Huang, S.G. Sun, J. Alloys Compd. 721 (2017) 229–235, https://doi.org/10.1016/j.jallcom.2017.05.305.
[17] B. Jiang, C. Xu, C. Wu, L. Dong, J. Li, F. Kang, Electrochim. Acta 229 (2017) 422–428, https://doi.org/10.1016/j.electacta.2017.01.163.
[18] T.D. Gregory, R.J. Hoffman, R.C. Winterton, J. Electrochem. Soc. 137 (1990) 775–780, https://doi.org/10.1149/1.2086553.
[19] P. Novak, J. Disilvestro, J. Electrochem. Soc. 140 (1993) 140–144, https://doi.org/10.1149/1.2056075.
[20] N. Sa, H. Wang, D.L. Proffit, A.L. Lipson, B. Key, M. Liu, Z. Feng, T.T. Fister, Y. Ren, C.-J. Sun, J.T. Vaughey, P.A. Fenter, K.A. Persson, A.K. Burrell, J. Power Sources 323 (2016) 44–50, https://doi.org/10.1016/j.jpowsour.2016.05.028.
[21] W. Sun, F. Wang, S. Hou, C. Yang, X. Fan, Z. Ma, T. Gao, F. Han, R. Hu, M. Zhu, C. Wang, J. Am. Soc. 139 (2017) 9775–9778, https://doi.org/10.1021/jacs.7b04471.
[22] R. Zhang, X. Xu, K.-W. Nam, C. Ling, T.S. Arthur, W. Song, A.M. Knapp, S.N. Ehrlich, X.-Q. Yang, M. Matsui, Electrochem. Commun. 23 (2012) 110–113, https://doi.org/10.1016/j.elecom.2012.07.021.
[23] P. He, X. Zhang, Y.G. Wang, L. Cheng, Y.Y. Xia, J. Electrochem. Soc. 155 (2008) A144–A150, https://doi.org/10.1149/1.2815609.
[24] T. Abe, F. Sagane, M. Ohtsuka, Y. Iriyama, Z. Ogumi, J. Electrochem. Soc. 152 (2005) A2151–A2154, https://doi.org/10.1149/1.2042907.
[25] S. Kim, S. Lee, K.W. Nam, J. Shin, S.Y. Lim, W. Cho, K. Suzuki, Y. Oshima, M. Hirayama, R. Kanno, J.W. Choi, Chem. Mater. 28 (2016) 5488–5494, https://doi.org/10.1021/acs.chemmater.6b02083.
[26] E. Levi, Y. Gofer, D. Aurbach, Chem. Mater. 22 (2010) 860–868, https://doi.org/10.1021/cm9016497.
[27] J.W. Long, L.R. Qadir, R.M. Stroud, D.R. Rolison, J. Phys. Chem. B 105 (2001) 8712–8717, https://doi.org/10.1021/jp0112830.
[28] H. Pan, Y. Shao, P. Yan, Y. Cheng, K.S. Han, Z. Nie, C. Wang, J. Yang, X. Li, P. Bhattacharya, K.T. Mueller, J. Liu, Nat. Energy 1 (2016) 16039, , https://doi.org/10.1038/NENERGY.2016.39.
[29] Z.W. Chen, C.H. Shek, J.K.L. Lai, Appl. Phys. A Mater. Sci. Process. 80 (2005) 703–707, https://doi.org/10.1007/s00339-004-3089-9.
[30] W. Li, J. Shao, Q. Liu, X. Liu, X. Zhou, J. Hu, Electrochim. Acta 157 (2015) 108–114, https://doi.org/10.1016/j.electacta.2015.01.056.